CORRESPONDENCE

Comments on "How Does the Boundary Layer Contribute to Eyewall Replacement Cycles in Axisymmetric Tropical Cyclones?"

Michael T. Montgomery and Sergio F. Abarca

Naval Postgraduate School, Monterey, California

Roger K. Smith

Ludwig Maximilians University of Munich, Munich, Germany

Chun-Chieh Wu and Yi-Hsuan Huang

Department of Atmospheric Sciences, National Taiwan University, Taipei, Taiwan

1. Introduction

In a recent paper, Kepert (2013, hereafter K13) investigated the theoretical role of the boundary layer in eyewall replacement cycles. Specifically, he used a family of steady-state, axisymmetric hurricane boundary layer models to examine the boundary layer response to an imposed radial profile of tangential winds with two wind maxima. Based on these solutions, he proposed a new feedback mechanism for secondary eyewall formation (SEF) and pointed to the role of the underlying boundary layer dynamics in this process. Specifically, he proposed (abstract) that "the boundary layer contributes to the formation of outer eyewalls through a positive feedback among the local enhancement of the radial vorticity gradient, the frictional updraft, and convection," and concluded (section 6) that "supergradient flow . . . is not essential to SEF."

Quoting from K13 (section 6), the proposed contribution of the boundary layer to SEF is as follows:

- "Some process(es) act(s) to produce a localized increase in the vorticity of the gradient wind at several times the primary RMW [radius of maximum tangential wind; our insertion]. . . . This local vorticity

increase could be the result of an internal adjustment/redistribution (e.g., by vortex Rossby waves). . . . It could be due to any of several processes, and is beyond the scope of this study to determine which."

- "The BL [boundary layer; our insertion] processes described in sections 4 and 5a lead to an increased updraft near the vorticity maximum."

- "The enhanced local updraft causes *an increase in convection* [our emphasis] near the vorticity maximum. This enhanced convection causes the low-level vorticity near the convection to increase (e.g. Haynes and McIntyre 1987; Raymond and Jiang 1990; Tory et al. 2012)."

- "The convectively induced local concentration of vorticity further strengthens the radial vorticity gradient on the outer edge of the maximum, and hence the frictionally forced updraft. The interaction between the BL and convection thus creates a positive feedback that causes the secondary eyewall to continue to develop."

A schematic of the proposed four-step feedback mechanism is sketched in Fig. 1. The sketch does not reflect the first step by which "some process" elevates the vorticity of the gradient wind to initiate the feedback process. The referred updraft maximum is that of the Ekman-induced frictional updraft near the top of the hurricane boundary layer (see displayed equation below). The feedback mechanism presumes that the vorticity at the top of the boundary layer may be accurately

Corresponding author address: Dr. Michael Montgomery, Naval Postgraduate School, Root Hall, Department of Meteorology, 589 Dyer Road, Monterey, CA 93943.
E-mail: mtmontgo@nps.edu

Newly proposed feedback mechanism for SEF (K13, Sec. 6)

$$\left\langle W_{Ekman,Eq.(22),K13} \right\rangle \Big|_{BLtop} \uparrow$$

$$\frac{\partial}{\partial r}\left\langle \zeta_{gr} \right\rangle \Big|_{BLtop} \uparrow \qquad \left\langle convection \right\rangle \Big|_{int} \uparrow$$

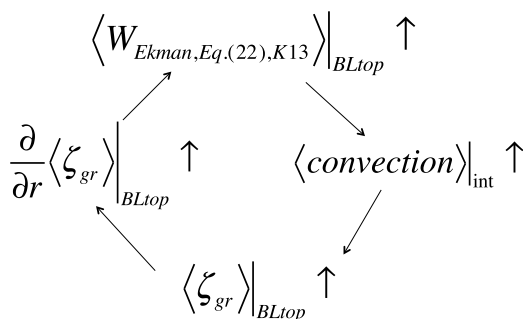$$\left\langle \zeta_{gr} \right\rangle \Big|_{BLtop} \uparrow$$

FIG. 1. Schematic diagram illustrating the new SEF feedback mechanism proposed in K13 (his section 6). In brief, an increase of the gradient wind vorticity (by some process not sketched, bottom of cartoon) near the top of the BL is argued to cause an increase in the magnitude of the radial vorticity gradient and the Ekman updraft velocity at the BL top. An increased Ekman updraft velocity is then presumed to result in an increase in the convection above the BL, an attending increase of the gradient vorticity at the BL top, a further strengthening of the corresponding radial vorticity gradient on the outer edge of the vorticity maximum, and so on. See text and/or K13 for more detailed description of the feedback loop. The angle brackets denote an azimuthal average of the corresponding quantity inside the brackets. The azimuthal average is to be carried out on a constant height surface. Equation (22) from K13 is reproduced here, for completeness, as the displayed equation in section 2.

represented using the gradient wind near the top of the boundary layer.

The reason for the present focus on the Ekman-like updraft in the proposed feedback loop (represented in Fig. 1) stems from section 5 of K13 entitled "Insights from linear Ekman theory" and the subsequent summary provided in section 6 entitled "Discussion: The role of the boundary layer in secondary eyewall formation" where the author states (p. 2828, right column) "...the approximate location and strength of the updraft are determined by *much simpler dynamics* [our emphasis], namely the near balance between radial advection and the surface sink of absolute angular momentum; while there are differences of detail between the models, they can be reasonably well predicted from the gradient wind alone. It is the location of the increased vorticity outside of the primary eyewall that determines where the outer frictional updraft forms."

In K13 (p. 2827, right column) the author states "One difference between the linear and nonlinear models is important to this hypothesis. The linear model locates the updraft on the region of enhanced vorticity gradient outside any local vorticity maximum, so the convectively generated vorticity will add to the outside [sic] the existing maximum and broaden rather than strengthen it. In contrast, the nonlinear model places the frictionally

forced updraft farther inward, so the vorticity generated by the enhanced convection will tend to strengthen, rather than broaden, the existing vorticity perturbation."

The nonlinear effects are, in the above quoted paragraph, simply contributing to a radially inward shift in the location of the frictionally forced updraft and corresponding vorticity enhancement at the top of the boundary layer. Other than these quantitative effects, the nonlinear boundary layer dynamics do not seem to be invoked in K13 to fundamentally alter the feedback process sketched above. There is a presumption also that the frictionally forced updraft will enhance the convection. The author of K13 does not state what he means by "enhanced convection." It would be natural to assume that this means that the buoyancy of convective updrafts would be increased. This issue will be discussed further in section 3.

2. Testing the proposed K13 feedback mechanism for SEF

The proposed SEF feedback mechanism summarized in Fig. 1 is scientifically interesting and invites scrutiny using observational data or established models. The subtle connection between the gradient wind at the top of the boundary layer, the corresponding vertical vorticity, and the induced-frictional updraft at this level presents many challenges for a test using observational data, not the least of which is the noisiness of the real wind data and even more so the corresponding vorticity data near the top of the boundary layer [see Marks et al. (2008), their Figs. 3b and 13a, respectively]. In this note, we sidestep the challenge of testing the new hypothesis using observational data and choose instead tests using two independent cloud-representing numerical solutions of a mature tropical cyclone undergoing SEF. The first of these simulations is an integration of the Regional Atmospheric Modeling System (RAMS) model, described in Terwey and Montgomery (2008), Terwey et al. (2013), and Abarca and Montgomery (2013). This simulation employs the Louis boundary layer parameterization [Louis (1979), the scheme recommended by Kepert (2012)]. The second is one representative ensemble member of the control experiment of Wu et al. (2012), a dataset of the Weather Research and Forecasting (WRF) Model and ensemble Kalman filter (EnKF) data assimilation for Typhoon Sinlaku (2008). [The pathway to SEF associated with this representative ensemble member is proposed and investigated in Huang et al. (2012).] The WRF simulation uses the Yonsei University planetary boundary scheme (Hong et al. 2006).

Figures 2 and 3 show radius–height contour plots and radial profiles of the azimuthally and temporally averaged
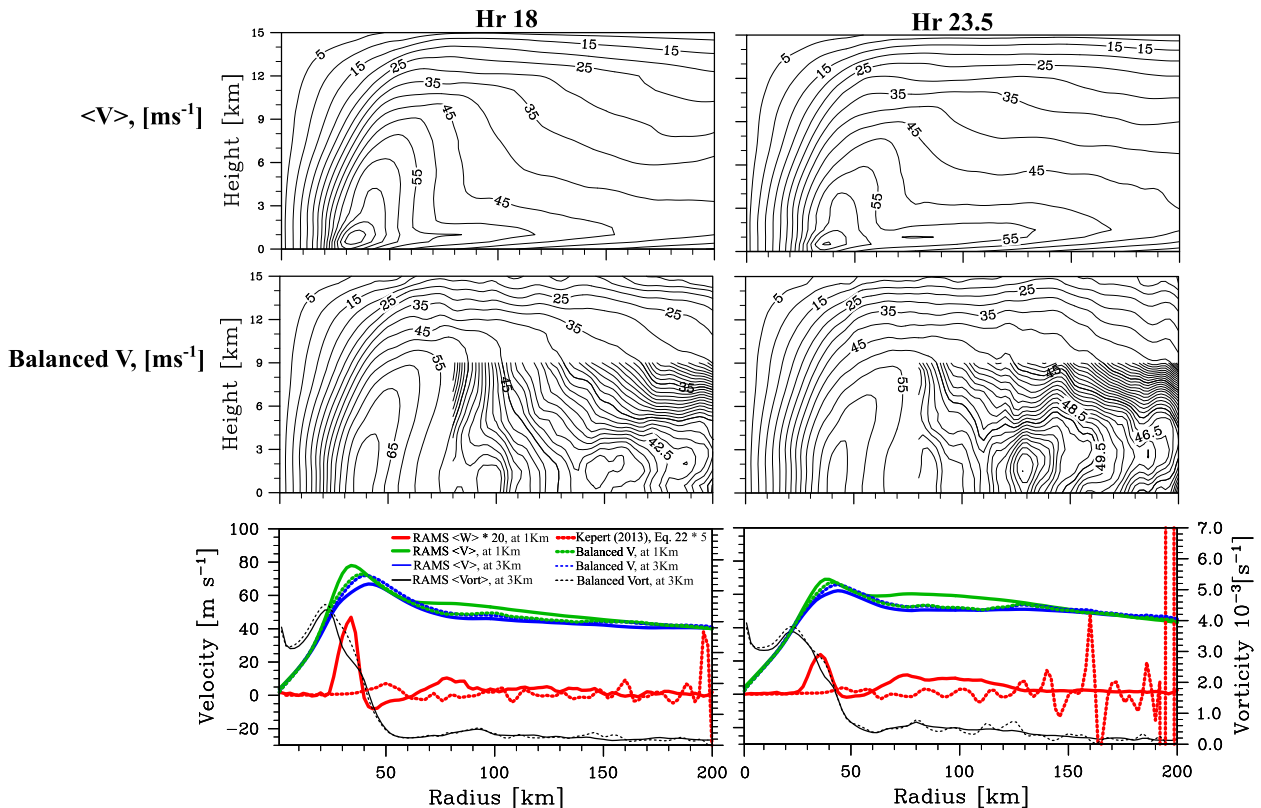
FIG. 2. (top) Radius–height plots of azimuthal- and time-averaged tangential velocity from the RAMS simulation undergoing SEF. (middle) Corresponding tangential wind field derived assuming gradient wind balance. (bottom) Radial profiles of the following flow quantities after azimuthal and time averaging: Ekman updraft velocity $\langle W\_Ekman \rangle$ [multiplied by 5, dashed red curve; obtained from Eq. (22) of K13 with the RAMS parameters at 3-km height to evaluate the balanced tangential wind above the boundary layer; see text for details], RAMS vertical velocity $\langle W \rangle$ at 1-km height (multiplied by 20, solid red curve), RAMS tangential velocity $\langle V \rangle$ at 1-km height (solid green curve), RAMS tangential velocity at 3-km height (solid blue curve), and RAMS relative vertical vorticity $\langle Vort \rangle$ at 3-km height (solid black curve). Shown for comparison is the corresponding gradient wind at 1-km height (dashed green curve) and 3-km height (dashed blue curve), as well as the corresponding relative vertical vorticity of the gradient wind at 3-km height (dashed black curve). The time averages are obtained using 1 h of data (output every 6 min), centered at the time indicated [(left) hour 18 and (right) hour 23.5]. Contours in the top two rows are every $5 \, \mathrm{m \, s^{-1}}$, except for radii $> 80 \, \mathrm{km}$ and height $< 9 \, \mathrm{km}$, where contours are shown every $0.5 \, \mathrm{m \, s^{-1}}$.

fields needed to assess the new SEF hypothesis summarized in Fig. 1. Note that we use a 1-h (arithmetic) average, although the original hypothesis does not make any additional assumptions of time (or space) filtering.[1] Figure 2 presents results from the RAMS integration, while Fig. 3 presents results from the WRF simulation. In the figures, the top rows show radius–height cross sections of azimuthal- and time-averaged tangential velocity. The second rows show the corresponding tangential wind field derived assuming gradient wind balance, computed as in Holton (2004, his

chapter 3), using the azimuthal- and time-averaged radial pressure gradient force per unit mass.[2] The bottom rows show radial profiles of several pertinent quantities at the height of 1 and 3 km. In both simulations, the 1-km height is within the boundary layer (near its top) and roughly corresponds to the height at which the secondary tangential wind maximum emerges (top row, right in Figs. 2 and 3). To be consistent with the intent of the K13 hypothesis, the 3-km height is used to deduce the gradient wind (analogous to flight level from reconnaissance aircraft) since the tangential winds are

---

[1] Results derived using no time averaging (not shown) lead to the same conclusions presented here. Further manipulation or filtering of the model data is not carried out so as to preserve the scientific integrity of the model data.

[2] This computation requires the solution of a quadratic formula. In the dataset used, the radicand becomes negative in some sparse regions in the upper-tropospheric outflow layer. To avoid this problem, $\partial p / \partial r$ is set to zero locally when its value becomes negative.
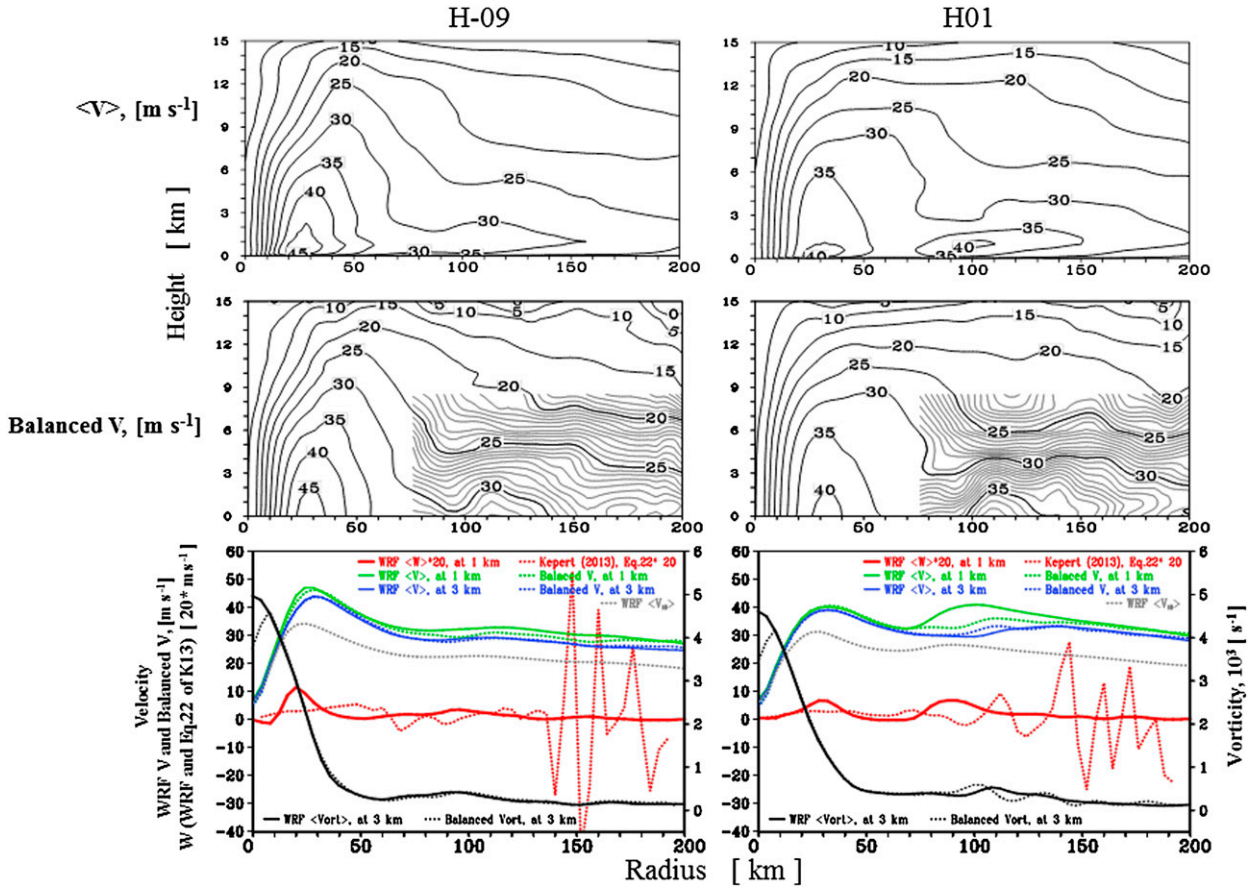
FIG. 3. As in Fig. 2, but for the WRF simulation and EnKF data assimilation result of CTL presented in Wu et al. (2012) and Huang et al. (2012). The 1-h average is evaluated by 2-min output data. H01 corresponds to 0800 UTC 11 Sep 2008, which is 1 h after the SEF time identified in Wu et al. (2012), while H-09 is 9 h prior to SEF. Note that the magnitude of WRF $\langle W \rangle$ at 1-km height and $\langle W \rangle$ evaluated by Eq. (22) of K13 are both multiplied by 20. The tangential wind at 10-m height, corresponding to the lowest model level for wind, is used to derive v' (departure from the gradient wind at 3-km height) in Eq. (22) of K13. (bottom) The radial profile of tangential wind at 10-m height is shown by the gray dashed curve.

still modestly supergradient at 1-km height. The radial profiles shown in the bottom rows depict the azimuthally and (1 h) time-averaged tangential velocity, absolute vorticity, and vertical velocity from RAMS (Fig. 2) and WRF (Fig. 3), as well as the corresponding gradient wind and gradient absolute vorticity. The green curves in the radial profile plots depict the pertinent model tangential velocity data at 1-km height, while the blue curves depict model tangential velocity data at 3-km height. The black curves show the vorticity profiles at 3-km height. Shown also in the bottom row is the azimuthally averaged vertical velocity at 1 km (red solid curve) and the frictional updraft velocity predicted from Eq. (22) of K13 (red dotted curve):

$$w_\infty = \frac{1}{r} \frac{\partial}{\partial r} \frac{rC_d V[V + 2v'(0)]}{\zeta_{\mathrm{gr}} + f},$$

where V is the gradient wind, ζ_{gr} is the relative vorticity of the gradient wind, $v'(0)$ is the departure from the tangential gradient flow, C_d is the drag coefficient, f is the Coriolis parameter, r represents radius, and $\partial/\partial r$ denotes the partial derivative with respect to r. To compute w_∞ in Fig. 2, the height of 3 km is taken as the gradient wind value (see discussion above). Also, as used in K13,[3] $C_d = 0.002$. Finally, following K13, $V + v'(0)$ is the azimuthal wind at the height where the drag coefficient is defined (nominally 10-m level). From Powell et al. (2009), $V + v'(0)$ is considered to be $0.84V$, from where it follows that $v'(0) = -0.16V$, and then $V + 2v'(0) = 0.68V$. The latter value is used in the evaluation of Eq. (22) of K13.

---

[3] The results presented here do not qualitatively change when using other common representations of C_d [e.g., Deacon's formula following Roll (1965)].

In the context of the proposed feedback loop (Fig. 1), Fig. 2 at 18 h (during SEF) shows that the locally negative radial vorticity gradient of the gradient wind at 3-km height (near 100-km radius, bottom row, left panel, dashed black curve) is accompanied by a locally positive frictional updraft maximum there (bottom row, left panel, dashed red curve). Following the argument of K13, this frictional updraft maximum would cause "an increase in the convection" (bullet point 3 in section 1) above the boundary layer near this radius and in turn an increase in the local radial gradient of vorticity (at the boundary layer top). The increased vorticity that results from this increased radial vorticity gradient is presumed to result in a local increase in the gradient wind and so on, culminating in a localized updraft and secondary eyewall near the radius of the heightened radial vorticity gradient of the gradient wind (we caution again that K13 does not elaborate on what is meant by "an increase in the convection," an aspect that is discussed further in items 2 and 4 in section 3).

Inspection of the individual panels that constitute both Figs. 2 and 3 indicate a quite different sequence of events than that proposed by K13. In Fig. 2, the top and middle rows show that the gradient wind has three discernible tangential wind maxima outside of the primary eyewall at both 18 and 23.5 h. In contrast, the RAMS data have no tangential wind maximum beyond the primary eyewall at 18 h and possess only one secondary tangential wind maximum at 23.5 h. In the bottom rows, a distinct secondary maximum of the gradient wind at 23.5 h occurs near 130 km with a corresponding Ekman updraft exterior to 130-km radius in a series of positive and negative oscillations.[4] The most prominent secondary gradient wind maximum at 23.5 h (at 3-km height) is 30 km outside the secondary gradient wind maximum depicted 5 h earlier in the middle and bottom rows.

In contrast to the foregoing features associated with the gradient wind and related Ekman updraft, the corresponding RAMS data at 1-km height and at 18 h show that the mean updraft maximum is located at approximately 80 km and the tangential wind is nearly constant between 70 and 90 km. At hour 23.5, the primary eyewall's tangential wind maximum has diminished in intensity somewhat, but a radially broad secondary

tangential wind maximum, centered at approximately 80-km radius, has emerged. Also at this time, the mean updraft outside of the primary eyewall exhibits a maximum at approximately 75-km radius and has also a broad radial scale, consistent with the weakly organized convective activity in azimuth near this radius as shown in Terwey and Montgomery (2008, their Fig. 4).

Figure 3 shows results of the aforementioned WRF simulation and EnKF data assimilation described in Wu et al. (2012) and Huang et al. (2012) in a form similar to Fig. 2. The adopted planetary boundary layer scheme uses the friction velocity obtained by similarity theory to parameterize wind stress. To carry out the calculation of the frictionally forced mean updraft based on the linear Ekman theory [Eq. (22) of K13], C_d is retrieved via the relationship of $C_d = U^{*2}/\text{wspd}_{10}^2$ where U^* is the friction velocity defined in the similarity theory and wspd_{10} is the wind speed at 10-m height. The quantity $v'(0)$ above is evaluated directly by deducing wspd_{10} from the gradient wind at 3-km height. Similar to the RAMS results, a number of maxima in the balanced tangential wind (gradient wind) are distinct well before SEF, at least 9 h preceding SEF (middle row, left panel) when the tangential wind is broadening in the middle and lower troposphere (top row, left panel). At the moment when the secondary maximum in the tangential wind field becomes robust (H01: an hour after SEF), the secondary maximum in the balanced wind is less distinct in comparison with that of the tangential winds (right panel), indicating a significant contribution of the unbalanced flow to the wind maximum in the outer eyewall, particularly near the top of boundary layer inflow (~1-km height).

The frictionally forced vertical velocity, as proposed by K13 [his Eq. (22), bottom row, red dotted line] is inconsistent with that in the WRF simulation near the top of the boundary layer (about 1-km height in the SEF region). During the expansion of total tangential winds (e.g., at H-09; 9 h before SEF), multiple updrafts and downdrafts are evident at radii between 30 and 200 km (bottom row, left panel, red dotted line). In particular, this frictionally forced vertical velocity does not capture the double peaks of upward motion in the two eyewalls when the outer eyewall is present (e.g., at H01). At H01, the innermost maximum of the estimated frictional vertical velocity is located near $r = 70$ km, between the two WRF-simulated maxima. As for the secondary updraft structure, the WRF-simulated updraft is present around $80 < r < 100$ km, while multiple updrafts and downdrafts are depicted by the frictionally forced vertical velocity predicted by Eq. (22) of K13 outside of 100-km radius. The explanation for these unrealistic vertical velocity predictions is that the frictional vertical

---

[4] In Fig. 2, the azimuthally averaged Ekman vertical velocity is plotted with a scaling factor of 5 and the corresponding RAMS vertical velocity at the boundary layer top is plotted with a scaling factor of 20 so that the shape of the two radial profiles may be compared easily. In Fig. 3 (the upcoming WRF analyses), an identical scaling factor of 20 is employed for the Ekman and WRF model vertical velocities at the boundary layer top.

velocity evaluated by Eq. (22) of K13 is quite sensitive to small radial gradients of the gradient wind and its associated vorticity in the region where the absolute vorticity is small. This is a conclusion of the present note; it was not foreseen in K13. Thus, Eq. (22) of K13 tends to predict synthetic pairs of updraft and downdraft from given vortex profiles of the cloud-resolving model or observations with the nature of small fluctuating features.

3. What are the limitations of the K13 hypothesis?

To understand why the K13 hypothesis is not supported by the two independent full-physics hurricane simulation data considered here, it is necessary to review the basis for the hypothesis, which was arrived at using theoretical reasoning and the results of three steady-state, axisymmetric models of the hurricane boundary layer. These models are the linear analytical model of Kepert (2001), the nonlinear model of Kepert and Wang (2001) and Kepert (2012), and the boundary layer part of the three-layer axisymmetric hurricane model (Ooyama 1969). Such numerical models are used to diagnose the steady-state response of the boundary layer to an analytically prescribed, radial profile of vorticity at the top of the boundary layer with two associated vorticity maxima (K13's Figs. 1, 2, and 7–9). The supporting theoretical arguments are based mostly on linearized Ekman balance theory, which predicts the updraft strength at the top of the boundary layer in terms of the local values of the absolute vorticity (using the gradient wind) and its radial gradient at the top of the boundary layer.

We have a number of concerns with the reasoning presented and theoretical steps taken by K13 as detailed below:

1) We are puzzled about K13's predictions of secondary eyewall formation based on a set of equations that do not contain time derivatives. (Each of the three models presented in K13 solve steady-state boundary layer equations.)

2) K13 proposes a local feedback between the frictionally induced inflow and convection, although he does not elaborate on the precise aspects of the convection he has in mind (e.g., upward mass flux, diabatic heating rate, updraft buoyancy). It is certainly physically incorrect to assume that all the mass that converges in the boundary layer can be ventilated by the convection, since the ability of the convection to ventilate the converged mass depends, inter alia, on the buoyancy of the convective updrafts, which, in turn, depends on the thermodynamic properties of the converged air in relation to the moist convective

stability of the air in the vortex aloft. Also, the vertical mass flux out of the boundary layer does not determine the diabatic heating rate within deep convection or the radial gradient of this heating rate. However, it is precisely this radial gradient and its vertical profile that would primarily determine the axisymmetric balance response of the vortex above the boundary layer (e.g., Bui et al. 2009 and references therein). In brief, one cannot realistically discuss a feedback with convection without considering a model or parameterization of convection. Indeed, different convective parameterizations can lead to quite different outcomes (see, e.g., Zhu et al. 2001) and one closure on cloud base mass flux that sets it equal to the mass convergence in the boundary layer is known to be unrealistic (Raymond and Emanuel 1993). For one thing, such a closure ignores all between-cloud subsidence into the boundary layer. This is a pertinent issue in the outer eyewall region, where the convection is more diffuse and not ringlike in the early stage of SEF (Terwey and Montgomery 2008, their Fig. 4; Wu et al. 2012, their Fig. 8).

3) The linearized, Ekman-like balance formulation of the boundary layer that is the theoretical basis of the K13 hypothesis (his section 5 and beginning of section 6) is not valid when the local vortex Rossby number $R_o \sim O(1)$ [see Smith and Montgomery (2008), their Eq. (16), for the definition of the appropriate vortex Rossby number and related discussion for a slab approximation and Vogl and Smith (2009), their Figs. 5 and 6, demonstrating that the linearized, Ekman-like balance approximation is inconsistent, because the nonlinear terms predicted using it are not small]. As an illustrative example, Fig. 4 demonstrates that R_o is of order unity in the radial region of SEF (between 75 and 100 km during 18–23 h), using the simulation studied extensively in Terwey and Montgomery (2008), Terwey et al. (2013), and Abarca and Montgomery (2013). Similarly, Fig. 5 shows R_o for the WRF simulation, demonstrating that in the SEF region (between 75 and 125 km) R_o lies in the range of 0.5 and 1.5 between times H-15 and H0. Since R_o is not much smaller than unity in the SEF region in both simulations, we conclude that advective departures from Ekman-like balance in the boundary layer and local time derivatives of the horizontal velocity cannot be neglected in general.

4) A further issue is that boundary layer theory formally breaks down in regions of deep convection owing to the horizontal pressure gradient induced in the boundary layer by the convection. As buoyant air rises in a deep convective updraft, boundary layer air is drawn toward the updraft. This "suction effect"
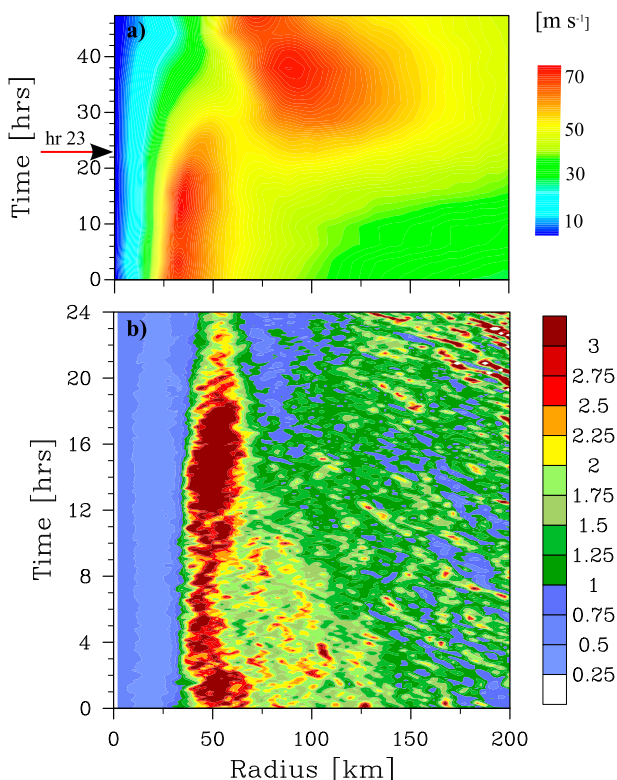
FIG. 4. Radius–time plot of azimuthally averaged (a) tangential wind velocity (at 1.5-km height; m s^{-1}) and (b) a local Rossby number as defined in Smith and Montgomery [2008, their Eq. (16)]. The local Rossby number is based on the boundary layer–averaged, storm-relative tangential velocity. [For reference, hour 23 is indicated in (a) and corresponds to the time of the earliest tangential velocity secondary maximum near 1-km height (see Fig. 1).]

cannot be described by boundary layer equations as their parabolic nature precludes their knowledge of flow properties in the downstream direction (i.e., information is conveyed in the direction of flow only). It certainly cannot be described by the local Ekman solution. Indeed, evidence for this suction effect during SEF can be inferred from Fig. 7c of Huang et al. (2012), which shows that the radial pressure gradient force per unit mass in the SEF region decreases approximately linearly with height from the lower surface as the secondary eyewall forms. Our point is that, in general, the upflow generated with the boundary layer model cannot be expected to match that which is diagnosed by the three-dimensional model because the boundary layer model knows nothing about the convectively induced radial pressure gradient in the boundary layer.

In addition to the issues raised above, we find that K13 provides an inaccurate portrayal of the new paradigm of

tropical cyclone intensification presented in Smith et al. (2009) [further elaborated in Montgomery and Smith (2014)] to explain SEF in the studies by Huang et al. (2012) and Abarca and Montgomery (2013). Specifically, K13 (section 6) states the following: "Huang et al. attributes SEF exclusively to BL [boundary layer; our insertion] processes..." and "They [Huang et al. (2012)] attribute the development of the enhanced updraft to supergradient flow." We note here that Huang et al. (2012) [and Abarca and Montgomery (2013)] did present evidence in support of the idea that secondary eyewalls form via a progressive boundary layer control of the vortex dynamics in response to a radial broadening of the tangential wind field (as correctly cited in the introduction of K13). However, the application of the new overarching paradigm of tropical cyclone intensification to explain SEF does not attribute the formation process exclusively to the boundary layer. Also, Huang et al. (2012) did not refer to "enhanced updraft" to explain the SEF mechanism. Rather, they link the boundary layer dynamics with the region of increased frictional convergence outside of the primary eyewall together with the presence of convective instability there (see section 4).

4. How does the boundary layer contribute to SEF?

The precise explanation for the role of the boundary layer in SEF given by Huang et al. (2012, p. 668) was as follows: "The stronger and persistent boundary layer convergence within the SEF region (between 2100 UTC 10 September and 0300 UTC 11 September) implies that inflowing rings of air will be forcibly lifted out of the boundary layer to initiate and sustain deep convection in regions of convective instability. ... Given favorable local conditions, this forced ascent induced by the boundary layer dynamics (Fig. 4h) acts to sustain an approximate ring of deep convection within the SEF region."

In his appraisal of the role of the boundary layer in the proposed SEF feedback process, K13 (section 6) stated "We agree with much of the analysis regarding the radial momentum budget [of Huang et al. (2012); our insertion], and note that the analyses of the flow in Typhoon Sinlaku by them and Wu et al. (2012) are qualitatively similar to our idealized diagnostic calculations." K13 notes that "the nonlinear processes they discussed are present in our nonlinear model, where they contribute to important details of the flow such as the strong supergradient jet, the outflow above the jet, and the inward displacement and outward tilt of the updraft (relative to the linear model)." However, as highlighted in the introduction of this note, K13 goes on to state that "the approximate location and strength of
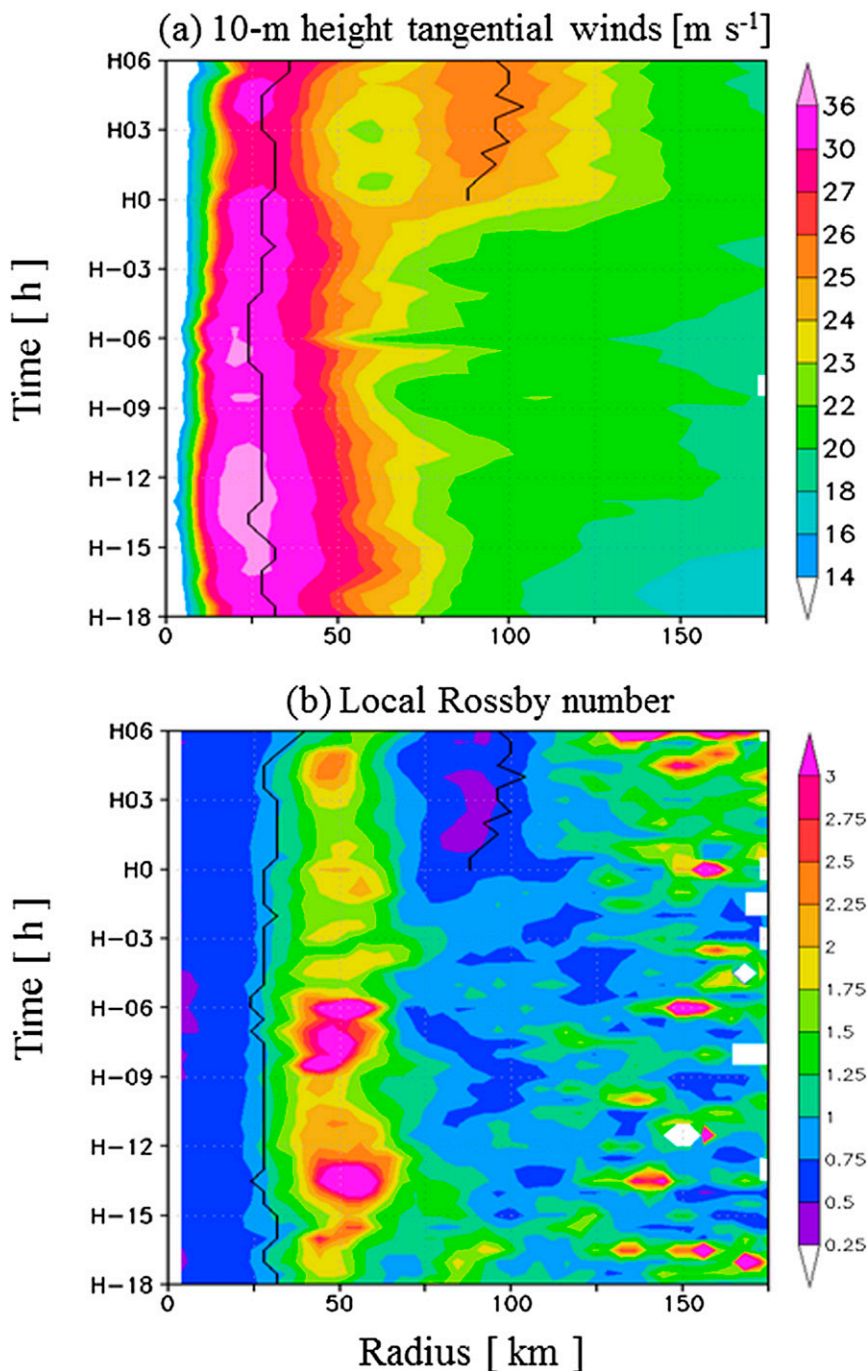
(a) 10-m height tangential winds [m s⁻¹]

(b) Local Rossby number

FIG. 5. Radius–time plot of azimuthally averaged (a) tangential wind velocity (at 10-m height; m s⁻¹), the quantity used to define SEF in Wu et al. (2012) and Huang et al. (2012), and (b) as in Fig. 4b, showing the local Rossby number. Two black lines on each subplot indicate the two radii of the local maximum tangential wind at 10-m height. Ordinate shows the hour relative to SEF. For instance, H0 is for the SEF time, H-01 stands for 1 h before SEF, and H01 indicates 1 h after SEF.

the updraft are determined by *much simpler dynamics* [our emphasis], namely the near balance between radial advection and the surface sink of absolute angular momentum; while there are differences of detail between

the models, they can be reasonably well predicted from the gradient wind alone. It is the location of the increased vorticity outside of the primary eyewall that determines where the outer frictional updraft forms.''

The evidence presented in section 2 demonstrates that the gradient wind and pertinent derived quantities from the linearized, Ekman-like balance formulation [Eq. (22) of K13] incorrectly predicts the location and strength of the updraft at the top of the boundary layer (~1-km height) in two independent mesoscale models undergoing SEF. The implication of this finding, together with the foregoing discussion, is that the nonlinear terms, the coupling of the boundary layer processes with the interior flow, and the local time derivatives of the horizontal velocity in the boundary layer should be accounted for to correctly capture the SEF dynamics as demonstrated in Huang et al. (2012) and Abarca and Montgomery (2013).

5. Conclusions

In this note we have examined the new hypothesis for secondary eyewall formation proposed by K13. The K13 hypothesis surmises that the boundary layer contributes to the formation of outer eyewalls through a positive feedback between the local enhancement of the radial vorticity gradient of the gradient wind near the top of the boundary layer, the frictional updraft, and convection. The hypothesis has been tested using two mesoscale model simulations (one with RAMS and the other with WRF) of secondary eyewall formation. It is shown to be unsupported by the results of these simulations. A careful examination of the hypothesis reveals four significant limitations, summarized briefly as follows: 1) the K13 hypothesis is based on a set of partial differential equations that does not contain time derivatives and thus is intrinsically unable to predict the future state of the flow, 2) deep convection is not determined generally by the Ekman convergence in the boundary layer, 3) the linearized Ekman balance formulation that is a foundation of the proposed SEF feedback mechanism cannot be justified when the local vortex Rossby number is of order unity—as is demonstrated by the full-physics mesoscale simulations, and 4) the boundary layer approximation formally breaks down in regions of deep convection.

K13 concluded (section 6) that "supergradient flow . . . is not essential to SEF." Given the limitations summarized above regarding the K13 predictions using two independent mesoscale models, it would seem difficult to maintain any claim regarding the unessential role of supergradient winds in the secondary eyewall formation process using a steady-state formulation.

REFERENCES

Abarca, S. F., and M. T. Montgomery, 2013: Essential dynamics of secondary eyewall formation. *J. Atmos. Sci.,* **70,** 3216–3230, doi:10.1175/JAS-D-12-0318.1.

Bui, H. H., R. K. Smith, M. T. Montgomery, and J. Peng, 2009: Balanced and unbalanced aspects of tropical-cyclone intensification. *Quart. J. Roy. Meteor. Soc.,* **135,** 1715–1731, doi:10.1002/qj.502.

Haynes, P. H., and M. E. McIntyre, 1987: On the evolution of vorticity and potential vorticity in the presence of diabatic heating and frictional or other forces. *J. Atmos. Sci.,* **44,** 828–841, doi:10.1175/1520-0469(1987)044<0828:OTEOVA>2.0.CO;2.

Holton, J. R., 2004: *An Introduction to Dynamic Meteorology.* 4th ed. Academic Press, 529 pp.

Hong, S.-Y., Y. Noh, and J. Dudhia, 2006: A new vertical diffusion package with an explicit treatment of entrainment processes. *Mon. Wea. Rev.,* **134,** 2318–2341, doi:10.1175/MWR3199.1.

Huang, Y.-H., M. T. Montgomery, and C.-C. Wu, 2012: Concentric eyewall formation in typhoon Sinlaku (2008). Part II: Axisymmetric dynamical processes. *J. Atmos. Sci.,* **69,** 662–674, doi:10.1175/JAS-D-11-0114.1.

Kepert, J. D., 2001: The dynamics of boundary layer jets within the tropical cyclone core. Part I: Linear theory. *J. Atmos. Sci.,* **58,** 2469–2484, doi:10.1175/1520-0469(2001)058<2469:TDOBLJ>2.0.CO;2.

——, 2012: Choosing a boundary layer parameterization for tropical cyclone modeling. *Mon. Wea. Rev.,* **140,** 1427–1445, doi:10.1175/MWR-D-11-00217.1.

——, 2013: How does the boundary layer contribute to eyewall replacement cycles in axisymmetric tropical cyclones? *J. Atmos. Sci.,* **70,** 2808–2830, doi:10.1175/JAS-D-13-046.1.

——, and Y. Wang, 2001: The dynamics of boundary layer jets within the tropical cyclone core. Part II: Nonlinear enhancement. *J. Atmos. Sci.,* **58,** 2485–2501, doi:10.1175/1520-0469(2001)058<2485:TDOBLJ>2.0.CO;2.

Louis, J. F., 1979: A parametric model of vertical eddy fluxes in the atmosphere. *Bound.-Layer Meteor.,* **17,** 187–202, doi:10.1007/BF00117978.

Marks, F. D., P. G. Black, M. T. Montgomery, and R. W. Burpee, 2008: Structure of the eye and eyewall of Hurricane Hugo (1989). *Mon. Wea. Rev.,* **136,** 1237–1259, doi:10.1175/2007MWR2073.1.

Montgomery, M. T., and R. K. Smith, 2014: Paradigms for tropical-cyclone intensification. *Aust. Meteor. Oceanogr. J.,* in press.

Ooyama, K. V., 1969: Numerical simulation of the life cycle of tropical cyclones. *J. Atmos. Sci.,* **26,** 3–40, doi:10.1175/1520-0469(1969)026<0003:NSOTLC>2.0.CO;2.

Powell, M. D., E. W. Uhlhorn, and J. D. Kepert, 2009: Estimating maximum surface winds from hurricane reconnaissance measurements. *Wea. Forecasting,* **24,** 868–883, doi:10.1175/2008WAF2007087.1.

Raymond, D. J., and H. Jiang, 1990: A theory for long-lived convective systems. *J. Atmos. Sci.,* **47,** 3067–3077, doi:10.1175/1520-0469(1990)047<3067:ATFLLM>2.0.CO;2.

——, and K. A. Emanuel, 1993: The Kuo cumulus parameterization in the representation of cumulus convection in numerical models. *The Representation of Cumulus Convection in Numerical Models, Meteor. Monogr.,* No. 46, Amer. Meteor. Soc., 145–147.

Roll, H. U., 1965: *Physics of the Marine Atmosphere.* International Geophysical Series, Vol. 7, Academic Press, 426 pp.

Smith, R. K., and M. T. Montgomery, 2008: Balanced boundary layer models used in hurricane models. *Quart. J. Roy. Meteor. Soc.,* **134,** 1385–1395, doi:10.1002/qj.296.

——, ——, and N. Van Sang, 2009: Tropical cyclone spin-up revisited. *Quart. J. Roy. Meteor. Soc.,* **135,** 1321–1335, doi:10.1002/qj.428.

Terwey, W. D., and M. T. Montgomery, 2008: Secondary eyewall formation in two idealized, full-physics modeled hurricanes. *J. Geophys. Res.,* **113,** D12112, doi:10.1029/2007JD008897.

——, S. F. Abarca, and M. T. Montgomery, 2013: Comments on ''Convectively generated potential vorticity in rainbands and formation of the secondary eyewall in Hurricane Rita of 2005.'' *J. Atmos. Sci.,* **70,** 984–988, doi:10.1175/JAS-D-12-030.1.

Tory, K. J., J. D. Kepert, J. A. Sippel, and C. M. Nguyen, 2012: On the use of potential vorticity tendency equations for diagnosing atmospheric dynamics in numerical models. *J. Atmos. Sci.,* **69,** 942–960, doi:10.1175/JAS-D-10-05005.1.

Vogl, S., and R. K. Smith, 2009: Limitations of a linear model for the hurricane boundary layer. *Quart. J. Roy. Meteor. Soc.,* **135,** 839–850, doi:10.1002/qj.390.

Wu, C.-C., Y.-H. Huang, and G.-Y. Lien, 2012: Concentric eyewall formation in Typhoon Sinlaku (2008). Part I: Assimilation of T-PARC data based on the ensemble Kalman filter (EnKF). *Mon. Wea. Rev.,* **140,** 506–527, doi:10.1175/MWR-D-11-00057.1.

Zhu, H., R. K. Smith, and W. Ulrich, 2001: A minimal three-dimensional tropical cyclone model. *J. Atmos. Sci.,* **58,** 1924–1944, doi:10.1175/1520-0469(2001)058<1924:AMTDTC>2.0.CO;2.